Research Article **Open Access**

Ioannis Tsagrakis, Iason Konstantopoulos, Alexandros Sidiropoulos, and Elias C. Aifantis*

On certain applications of gradient nanochemomechanics: deformation and fracture of LIB and SGS

https://doi.org/10.1515/jmbm-2019-0009
Received Jul 5, 2019; accepted Aug 10, 2019

Abstract: The term gradient nano-chemo-mechanics was introduced to encompass models incorporating higher order couplings between deformation and chemistry at the nanoscale. Along these lines, the article first reviews the basics of a robust theoretical framework developed for such processes focusing on elasticity and diffusion. The classical laws for Hookean deformation and Fickean transport are modified to include extra Laplacian terms and corresponding internal lengths modeling nonlocal interactions. Then, special cases are considered to describe deformation and fracture aspects of new energy materials; namely Li-ion battery (LIB) nanostructured anodes and disclinated metallic microcrystals (DMC). Both of these material systems are characterized by a high degree of spatial gradient structures (SGS) with extended surface for energy storage and catalysis applications.

Keywords: Gradient elastodiffusion, nanostructured silicon anodes, hollow disclinated microcrystals

1 Introduction

The terms "nanomechanics" and "chemomechanics" were introduced by the last author in 1995 [1] and 1980 [2] to point out the need for extending existing continuum mechanics models to the nanoscale, as well as the need for developing coupled deformation-diffusion models when mechanical stress and chemistry are present on an equal footing. Recent advances on nanoscience and nanotechnology have tremendously accelerated the development of such models, mainly due to the exponential growth of sophisticated multiscale computer codes and corresponding laboratory probes enabling to compare theory, simulation, and experiment at the same scale of observation.

A most notable contribution was the extension of classical Hooke's law of elasticity to include an extra gradient term (the Laplacian of Hookean stress) multiplied by a corresponding internal length parameter to account for weak deformation nonlocality. The resulting model [3], commonly known as gradient elasticity (or GradEla model) was used to eliminate stress singularities in dislocation lines and crack tips, as well as to interpret size effects in elastic structural components, not captured by classical elasticity theory. A recent review with a long list of related references can be found in [4]. Along similar lines, the classical Fick's law of diffusion was extended to include an extra gradient term (the Laplacian of Fickean flux) multiplied by a corresponding internal length parameter to account for weak diffusion nonlocality. The resulting model [5], commonly known as higher order diffusion, was used to interpret experimental data for grain boundary diffusion and nanopolycrystals, not captured by classical diffusion theory. A recent review with a long list of related references can be found in [6].

The aforementioned models of gradient elasticity and higher order diffusion have not been sufficiently considered to address coupled deformation-diffusion problems at the nanoscale where the interaction between elastic internal lengths and diffusion internal lengths need to be accounted for. This issue becomes especially important in considering chemomechanical processes at small volumes, such as those occurring in microstructured components used in advanced applications for energy storage and catalysis devices. Such a coupled nanochemomechanics framework will be outlined here for chemoelastic deformations. It will be used then to discuss chemomechanical damage in rechargeable lithium-ion battery (LIB) nanostructured anodes, as well as deformation and fracture of pentagonal disclinated microcrystals (DMC). LIBs is an important class of advanced energy storage devices (ESD). DMCs is an important class of objects with extended sur-

Ioannis Tsagrakis, Iason Konstantopoulos, Alexandros Sidiropoulos: School of Engineering, Aristotle University of Thessaloniki, 54006 Thessaloniki, Greece
***Corresponding Author: Elias C. Aifantis:** School of Engineering, Aristotle University of Thessaloniki, 54006 Thessaloniki, Greece, E-mail: mom@mom.gen.auth.gr

face and spatially gradient structure (SGS). In this connection, it is noted that some background on related aspects can be found in published joint work by the first and the last authors [7–10].

The plan of the paper is as follows. In Section 2 a brief review of open problems in LIB anodes is presented and the same is done for SGS materials. In Section 3 the basics of gradient elasticity and higher order diffusion are presented, along with the governing equations accounting for higher order elastodiffusion couplings. In Section 4 representative results on both LIB and SGS chemomechanical aspects are presented. Finally, in Section 5 some closing remarks for this initial effort on modeling deformation and fracture in LIB and SGS components are given, along with some open remarks for future directions.

2 Open problems in LIB and SGS

(i) ***LIB Anodes:*** In Figure 1, a representative configuration of a LIB device is shown, along with electrochemical reactions taken place in the anodes and cathodes. Commercially available LIBs use graphite (C) as anode. Current battery developers focus on replacing C with Sn and Si which lead to higher capacities. In Figure 2, the cyclic response of nanostructured anodes and electron microscopy images are provided. It is noted, however, that during lithiation/delithiation the active nanoparticles (Si, Sn or Al) embedded in an inert matrix (C, ceramic or polymer) undergo large volumetric expansions/contractions (theoretically up to 400% for freely expanding and fully lithiated Si active particles) which result to fracture and capacity fade. These volume changes may be suppressed by reducing the size of active nanoparticles to prevent chemomechanical damage and capacity fade upon electrochemical cycling. Obviously, this is a size effect problem which can be conveniently addressed within the coupled nanochemomechanical framework outlined in Section 3. Some representative results of such considerations are provided in Section 4.

(ii) ***SGS Objects*****:** In Figure 3, various SGS objects as produced by electrodeposition under mechanical steering are presented. These structures are characterized by pentagonal symmetry (not predicted by classical crystallography) due to internal disclination effects that emerge during processing and result to an extended surface with unusually high chemical activity. In Figure 4, a pentagonal Cu microparticle is shown, along with an internal void revealed by etching. The pentagonal symmetry can be described in terms of a disclination defect in an initially solid microparticle, the stress field of which can act as a vacancy accumulator along the disclination line, resulting to the formation of an internal void. The competition of the stress field generated by the disclination and that due to the external surface can lead to a fracture criterion as shown in Figure 5 by using a previous purely classical elasticity framework. Again, this is a size effect problem which can be conveniently addressed within the coupled nanochemomechanical framework outlined in Section 3. Some representative examples of such considerations are provided in Section 4.

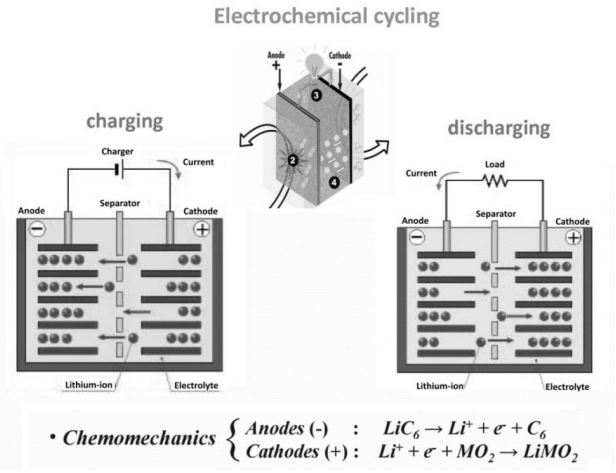

Figure 1: Typical electrochemical cell and Li reactions. Commercial graphite (C) is experimentally being replaced by Sn or Si. C gives a capacity of 370 mAh/g (LiC_6); Sn gives a capacity of 990 mAh/g ($Li_{4.4}Sn$) and Si gives a capacity of 4200 mAh/g ($Li_{4.4}Si$). The resulting volume expansion can reach 300-400%. [Courtesy of Katerina E. Aifantis]

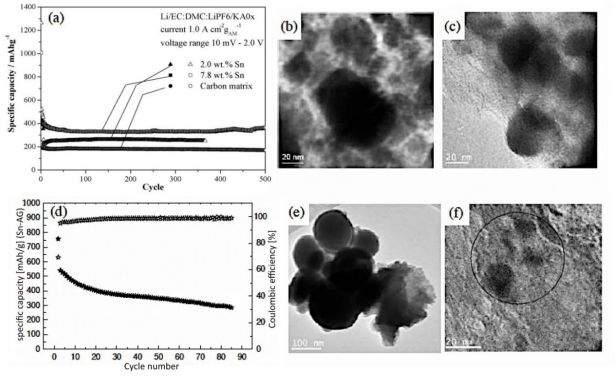

Figure 2: Volume fraction and size effects on capacity: (a) Capacity increase upon volume fraction increase of Sn content; (b) Corresponding Sn particles of size 20-50 nm before electrochemical cycling; (c) Mechanical stability of these particles after 80 cycles; (d) Capacity fade of larger Sn particles 100 nm as shown in (e), which fracture and delaminate into the electrolyte after 80 cycles as shown in (f). (Courtesy of K.E. Aifantis; see also K.E. Aifantis et al, *Electrochim. Acta* 2010 [22]; *J. Power Sources* 2012 [23]).

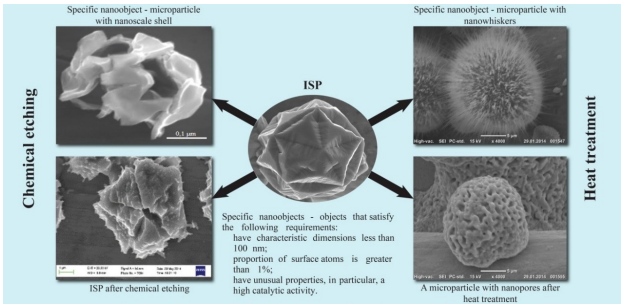

Figure 3: Various configurations of SGS objects produced by electrodeposition under mechanical steering. For a brief overview and related references the reader can consult [24] (E.C. Aifantis, *Rev. Adv. Mater. Sci.* 2017).

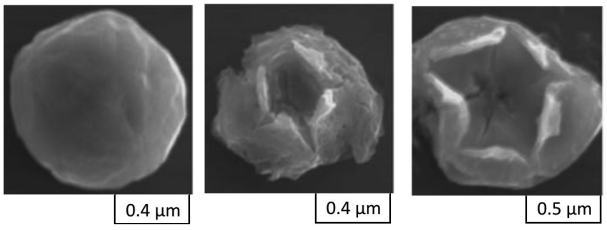

Figure 4: Cu micro/nanoparticle of pentagonal symmetry with an interior void revealed after chemical etching. For details, the reader can consult [10, 24] and references quoted therein.

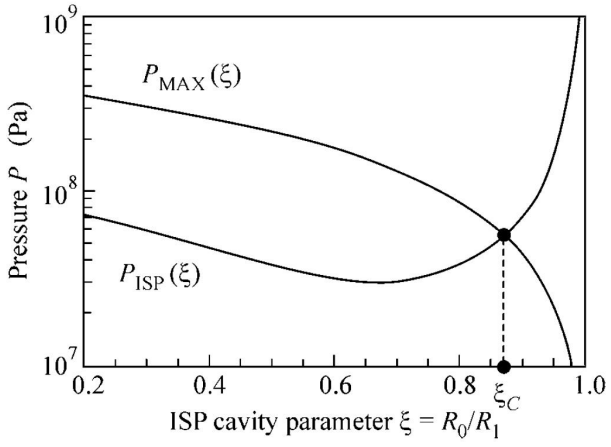

Figure 5: The critical parameter ξ (the ratio of the internal over external radius) of a hollow ISP particle as determined by classical elasticity theory. For details, the reader can consult [10, 20, 24] and references quoted therein.

3 Gradient elastodiffusion theory

For elastic deformations, the term $\ell_\varepsilon^2\nabla^2[\lambda\varepsilon_{mm}\delta_{ij} + 2G\varepsilon_{ij}]$ – where ℓ_ε denotes an elastic internal length (IL), ε_{ij} is the elastic strain, and (λ, G) are the Lamé constants – is incorporated into classical Hooke's law. Previous results (see [4] and references quoted therein) show that the resulting internal length gradient (ILG) model can eliminate stress/strain singularities from dislocation/disclination lines and crack tips and interpret elastic size effects. For elastic deformations at the atomic scale (near dislocation lines in crystals), ℓ_ε relates to the subatomic configuration and electronic state (through DFT calculations), while at the microscale ℓ_ε relates to particle size/spacing (through MD simulations). For diffusion problems the ILs enter through the additional term $\ell_d^2\nabla^2 j$, which generalizes the classical Fick's law (ℓ_d is a diffusional internal length and j denotes the diffusion flux), in a manner similar to the Cahn-Hilliard theory [11] for spinodal decomposition.

The above ideas can be extended in a straightforward manner for coupled elastodiffusion processes accounting for higher order internal length couplings. The standard equations that are usually employed to model coupled elasto-diffusion processes (without accounting for internal length couplings) are of the form $\sigma_{ij} = \lambda\varepsilon_{mm}\delta_{ij} + 2G\varepsilon_{ij} - \alpha\rho\delta_{ij}$, $j = -D\nabla\rho + M\rho\nabla\sigma_{ii}$ for the chemostress σ_{ij} and the mechanodiffusive flux j, where the coefficients (α, M) denote chemomechanical coupling constants and D is the diffusivity. The fields (ρ, ε_{ij}) denote concentration of the diffusing chemical agent and mechanical strain, respectively. Since these constitutive equations do not contain higher order ILs, related chemomechanical size effects and pattern formation may not be captured.

Within our Laplacian-based ILG formulation, it turns out that the above constitutive equations are generalized by replacing σ_{ij} with $\sigma_{ij} - \ell_\sigma^2\nabla^2\sigma_{ij}$; ε_{ij} with $\varepsilon_{ij} - \ell_\varepsilon^2\nabla^2\varepsilon_{ij}$; and ρ with $\rho - \ell_\rho^2\nabla^2\rho$, with $(\ell_\sigma/\ell_\varepsilon, \ell_\rho)$ denoting stress/strain and diffusional ILs. Under suitable assumptions, it is possible to uncouple the deformation and chemical fields by first computing a "ground" hydrostatic stress component σ_h^0 from a conventional or a gradient elasticity theory, and then derive the concentration ρ from a stress-assisted diffusion equation of the form $\partial\rho/\partial t = \left(D + N\sigma_h^0\right)\nabla^2\left[\rho - \ell_\rho^2\nabla^2\rho\right] - M\nabla\sigma_h^0\cdot\nabla\left[\rho - \ell_\rho^2\nabla^2\rho\right]$, where N is a new phenomenological constant accounting for the effect of hydrostatic stress on diffusivity. This model with $\ell_\rho = 0$ has been used extensively to model hydrogen embrittlement and stress corrosion cracking in metals [12], and it is compatible with a mechanodiffusive flux of the form $j = -\left(D + N\sigma_h^0\right)\nabla\rho + (M + N)\rho\nabla\sigma_h^0$ provided that $\nabla^2\sigma_h^0 = 0$. This constraint is removed here and the model is adopted to consider chemomechanical damage and failure in LIB anodes. As a "ground" hydrostatic stress, the constitutive equation $\sigma_h^0 = \sigma_{ij}\varepsilon_{ij}^0$ is used, where $\sigma_{ij} = \sigma_{ij}^c - \ell_\varepsilon^2\nabla^2\sigma_{ij}^c$; $\sigma_{ij}^c = \lambda\varepsilon_{mm}\delta_{ij} + 2G\varepsilon_{ij} - \alpha_{ij}\rho$; $\alpha_{ij} = \lambda\varepsilon_{mm}^0\delta_{ij} + 2G\varepsilon_{ij}^0$ and the tensor ε_{ij}^0 relates to the elastic misfit strains $\rho\varepsilon_{ij}^0$, which are assumed transversely isotropic for the Li/Si sys-

tem. In this connection, it is noted that for isotropic materials, α_{ij} reduces to $\alpha_{ij} = \alpha\delta_{ij}$ shown above in the standard form for the chemostress.

4 Benchmark problems for LIB & SGS

In this section, we present some results on model configurations pertaining to LIB nanostructured anodes and SGS pentagonal objects. We focus, in particular, on size effects in Si-nanowires (NWs) since these objects are currently explored as potential candidates for LIB anodes, as well as on size effects in hollow icosahedral small particles (ISPs) since these objects are currently explored as potential candidates for nanocatalysis.

(i) ***Size effect on failure of Si NW***: Failure during lithiation of a single Si nanowire has been addressed by developing a concentration-dependent modification of the so-called "universal fracture criterion" [13] to account for the strength decrease as the lithiation proceeds due to the weakening of Si-Si covalent bonding and the formation of metallic or mixed ionic-covalent bonds [14, 15]. An equivalent stress measure σ_{eq} has been defined for this criterion, with the onset of failure corresponding to values $\sigma_{eq}/\tau_0 \geq 1$. The quantity τ_0 is given by $\tau_0 = \alpha\sigma_T^F$, where the intrinsic parameter α depends on the compression-tension strength ratio σ_C^F/σ_T^F. This ratio varies as a linear function of Li concentration between the values $\alpha \cong 3.59$ for $\rho = 0$ and $\alpha = 1$ for $\rho = 1$ with the latter corresponding to the boundary between metallic and ionic or covalent bonding (see Figure 4 in [13]). For the tensile strength, the theoretical limit approximation $\sigma_T^F \cong E/10$ is adopted and the dependence of σ_T^F on lithium concentration is incorporated by employing the linear rule of mixtures $E(\rho) = E_0\left(1 - f(\rho)\right) + E_1 f(\rho)$, where $E_0 \cong 156$ GPa, $E_1 \cong 67$ GPa are the Young's modulus values found in [15] for Si and $Li_{4.4}Si$, respectively. Moreover, $f(\rho) = \upsilon\rho/(\upsilon\rho + 1 - \rho)$ is the volume fraction with $\upsilon \cong 4.4$ denoting the molar volume ratio between the fully lithiated and the unlithiated phase.

It has been found that smaller specimens exhibit lower equivalent stresses during the entire lithiation process, i.e. they are less susceptible to failure (Figure 6). More important, there is a critical value $\left(d/\ell_\varepsilon\right)_{cr} \cong 8.5$ at which the ratio $\max(\sigma_{eq})/\tau_o$ becomes smaller than 1 and thus, the theoretical limit fracture level is suppressed. Employing the value $\ell_\varepsilon \cong 0.94$ nm, which is estimated by fitting the predictions of the model to experimental results on the thickness of the lithiated/unlithiated Si interface, a critical specimen diameter $d_{cr} \cong 8$ nm is obtained, which is quite small (~19 times the Van der Waals diameter of silicon atoms).

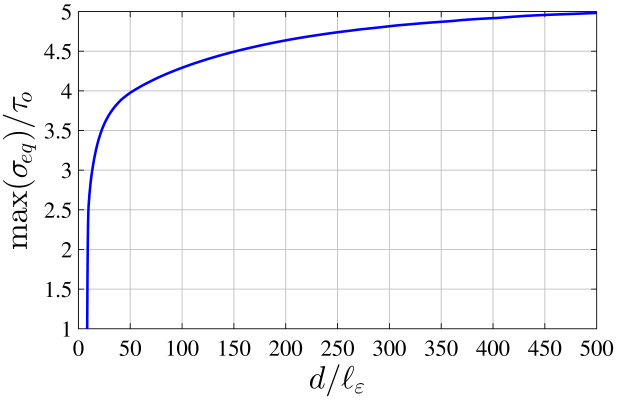

Figure 6: Size effect exhibited by the global maximum $\max(\sigma_{eq})$ that appears over the entire lithiation process.

Following the same procedure used for single silicon specimens, the theoretical failure stress of the active material in a nanocomposite anode made of silicon nanowires (active sites) of diameter d_{Si} embedded in a glass matrix can be estimated. In the absence of any data concerning the elastic internal length ℓ_m of the matrix, the inactive material is assumed to obey classical linear elasticity, i.e. $\ell_m = 0$.

The maximum equivalent stress for the entire lithiation process does not only depend on the ratio d_{Si}/ℓ_ϵ, but also on the ratio d_m/d_{Si} between the diameters of the unit cell and the active site which, in turn, is directly related to the density of silicon nanowires in the nanocomposite material. More important, as shown in Figure 7, the critical value $(d_{Si}/\ell_\epsilon)_{cr}$ for fracture suppression is quite larger than that of a free expanding nanowire and it is increased as d_m/d_{Si} is decreased, i.e. the density of the active sites becomes larger. Employing the aforementioned value of $\ell_\epsilon \cong 0.94$ nm, it gives a range between $(d_{Si})_{cr} \cong 23.5$ nm for $d_m/d_{Si} = 10$ and $(d_{Si})_{cr} \cong 65.5$ nm as $d_m/d_{Si} \to 1$. It is noted that while theoretical fracture of silicon is suppressed for any pair of values below the curves of Figure 7, the failure of both the active site and the glass matrix is suppressed only in the grey region thereof. This gives a minimum value of ~44% for the Si volume fraction in the closest (hexagonal) packing arrangement of the unit cells, combined with a maximum of $d_{Si} \sim 43$ nm.

(ii) ***Size effect on failure of a hollow Cu ISP*:** In this section, a stress gradient model of the form $\boldsymbol{\sigma} - \ell^2\nabla^2\boldsymbol{\sigma} = \boldsymbol{\sigma}^c$ is employed to discuss size effects occurring during the fracture of hollow ISPs produced by electrodeposition under mechanical steering. Under radial symmetry, this leads to the following differential equations for the components σ_{rr}

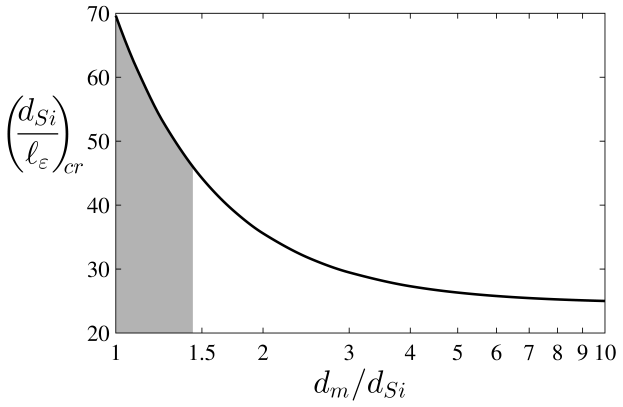

(a)

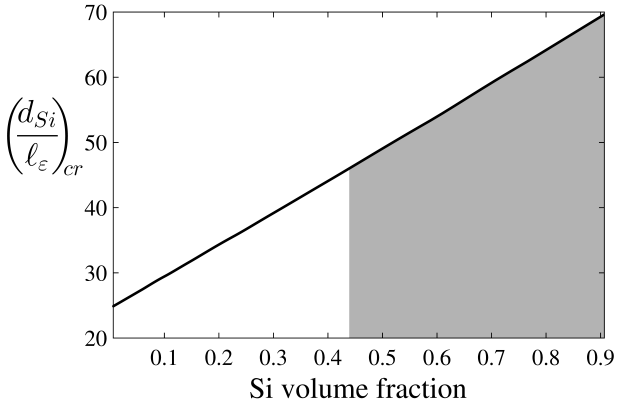

(b)

Figure 7: Critical ratio $(d_{Si}/\ell_\varepsilon)_{cr}$ between the diameter of the silicon nanowire and the elastic internal length for the suppression of the theoretical fracture of Si vs. (a) the ratio of the unit cell diameter over active site diameter, and (b) the volume fraction of silicon in the nanocomposite for the densest unit cell packing possible. The grey regions indicate suppression of fracture for both the active site and the glass matrix.

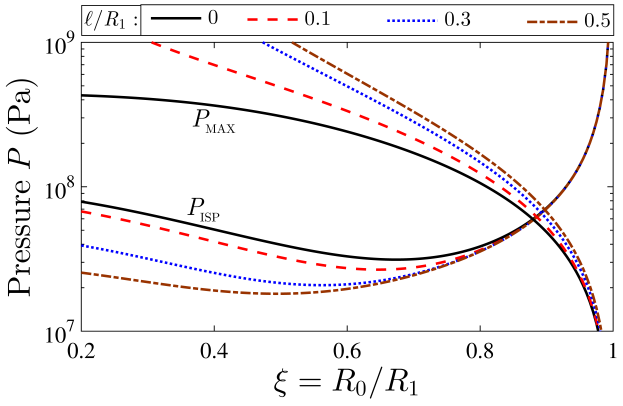

Figure 8: Stress gradient effects on the functions $P_{ISP}(\xi)$ and $P_{MAX}(\xi)$.

and $\sigma_{\theta\theta} = \sigma_{\varphi\varphi}$

$$\begin{aligned} \sigma_{rr} - \ell^2 \left(\frac{d^2\sigma_{rr}}{dr^2} + \frac{2}{r}\frac{d\sigma_{rr}}{dr} - \frac{4(\sigma_{rr}-\sigma_{\theta\theta})}{r^2} \right) &= \sigma^c_{rr}, \\ \sigma_{\theta\theta} - \ell^2 \left(\frac{d^2\sigma_{\theta\theta}}{dr^2} + \frac{2}{r}\frac{d\sigma_{\theta\theta}}{dr} + \frac{2(\sigma_{rr}-\sigma_{\theta\theta})}{r^2} \right) &= \sigma^c_{\theta\theta}. \end{aligned} \quad . \tag{1}$$

This system is solved for a hollow disclinated ISP, as well as for a spherical shell subjected to uniform internal pressure P. For the former, the classical elastic stress field reads [16]

$$\begin{aligned} \sigma^c_{rr} &= \frac{4G\kappa}{3}\frac{1+\nu}{1-\nu}\left[\ln\left(\frac{r}{R_1}\right) + \frac{r^3-R_1^3}{R_1^3-R_0^3}\frac{R_0^3}{r^3}\ln\left(\frac{R_0}{R_1}\right)\right], \\ \sigma^c_{\theta\theta} &= \frac{4G\kappa}{3}\frac{1+\nu}{1-\nu}\left[\frac{1}{2} + \ln\left(\frac{r}{R_1}\right) + \frac{2r^3+R_1^3}{R_1^3-R_0^3}\frac{R_0^3}{2r^3}\ln\left(\frac{R_0}{R_1}\right)\right], \end{aligned} \tag{2}$$

where κ is the power of the Marks-Yoffe disclination, G is the elastic shear modulus, ν is the Poisson's ratio, R_1 is the outer radius of the particle and R_0 is the radius of the void. For an internally pressurized spherical shell the respective classical field reads

$$\sigma^c_{rr} = -P\frac{R_1^3 - r^3}{R_1^3 - R_0^3}\frac{R_0^3}{r^3}, \qquad \sigma^c_{\theta\theta} = P\frac{2r^3 + R_1^3}{R_1^3 - R_0^3}\frac{R_0^3}{2r^3}. \tag{3}$$

For both problems, the homogeneous natural boundary condition $\partial_n \boldsymbol{\sigma} := \sigma_{ij,m} n_m = 0$ is taken at the inner and outer surfaces. This choice is the most widely used when dealing with gradient elasticity [17, 18]. The same boundary condition has been assumed in [19] by employing suitable thermodynamics arguments for the Eringen's nonlocal elasticity or stress gradient model. In this connection, it is noted that this differs from the conditions employed in [10] to determine the stress profiles for both solid and hollow ISP.

The derived solutions of Eq. (1) are not provided here due to their complicated form but in both cases, they can be recast into the forms $\sigma_{rr} = \sigma^c_{rr} + \sigma^g_{rr}$, $\sigma_{\theta\theta} = \sigma^c_{\theta\theta} + \sigma^g_{\theta\theta}$. As shown in [10], these, in turn, lead to the following expression for the total energy of an ISP with a void in its center

$$\begin{aligned} E_{ISP} = 4\pi\gamma(R_0^2 + R_1^2) + \frac{8\pi G\kappa^2(1+\nu)}{27(1-\nu)} \\ \left[R_1^3 - R_0^3 - \frac{9R_0^3R_1^3}{R_1^3 - R_0^3}\left(\ln\left(\frac{R_0}{R_1}\right)\right)^2\right] + E^g_d, \end{aligned} \tag{4}$$

where γ is the surface energy of the material and E^g_d is the part of the strain energy introduced by the presence of the gradient term in the constitutive equation. For the aforementioned homogeneous boundary condition, E^g_d may be calculated from the relation

$$E^g_d = 2\pi \int_{R_0}^{R_1} \left(\sigma^g_{rr}\varepsilon^c_{rr} + 2\sigma^g_{\theta\theta}\varepsilon^c_{\theta\theta}\right) r^2 dr, \tag{5}$$

where ε^c_{rr}, $\varepsilon^c_{\theta\theta}$ is the classical strain field.

Following a similar analysis with that given in [20] in the framework of classical elasticity, the pressure on the inner surface of the ISP particle may be calculated by using the relation $P_{ISP} = E_{ISP}/V$, where $V = \frac{4}{3}\pi(R_1^3 - R_0^3)$ is its volume. The respective pressure P_{MAX} at the point of fracture is determined by the solution of Eq. (1) for the internally pressurized shell, yielding

$$P_{MAX} = \frac{\sigma}{\frac{2\xi^3+1}{2(1-\xi^3)} + C_1(\bar{\ell},\xi)\hat{I}_{\frac{5}{2}}(\xi/\bar{\ell}) + C_2(\bar{\ell},\xi)\hat{I}_{-\frac{5}{2}}(\xi/\bar{\ell})}, \quad (6)$$

where σ is the ultimate stress of the material making up the spherical shell and $\xi := R_0/R_1$, $\bar{\ell} := \ell/R_1$, while $\hat{I}_{n/2}(x) := \sqrt{\pi/2x}I_{n/2}(x)$ with $I_{n/2}(x)$ denoting the respective modified Bessel functions. Moreover, $C_1(\bar{\ell},\xi)$ and $C_2(\bar{\ell},\xi)$ are integration constants determined by the aforementioned boundary conditions but they are not given here due to their lengthy form. It is also noted that unlike [20], the thick-shell solution has been adopted here rather than its thin-shell simplification.

For electrolytic copper the material parameters found in [20] have been used apart from κ which has been misprinted therein although the approximation $\kappa = 0.06$ of the correct value $\kappa = 0.0615$ [21] has been used in their calculations. In Figure 8, the functions $P_{ISP}(\xi)$ and $P_{MAX}(\xi)$ for different internal over geometrical length ratios $\bar{\ell} := \ell/R_1$ are depicted. As shown, larger gradient effects (i.e. greater $\bar{\ell}$ values) lead to larger ξ_c values at the point of fracture $P_{ISP} = P_{MAX}$ and thus, larger voids are attainable.

5 Conclusions

A preliminary effort has been described to show that coupled chemomechanical models are necessary to model elastodiffusion processes in small volume material components used in current energy storage and catalysis technologies. The focus was on nanostructured LIB anodes and SGS objects with pentagonal symmetry. The results indicate that such models can capture size effects that are observed in these components and can potentially lead to protocols and design criteria to prevent failure and optimize their performance in related applications.

Acknowledgements: The support of NSRF 2014 – 2020 for the project MIS 5005134: "*Nano-chemomechanics in Deformation and Fracture: Theory and Applications in LIBs and SGS*" is acknowledged. Problem identification and formulation of the general framework was due to ECA, while certain aspects on its implementation in the benchmark studies and most calculations were performed by IT. IK has rechecked these calculations and performed additional ones for other variants of the presently discussed DMC models that will be included in a separate publication. Finally, AS was included in the original research team for the project with the expectation to compare the theoretical results obtained herein with experiments.

References

[1] Aifantis E.C., In: 2nd International Symposium on Microstructures and Mechanical Properties of New Engineering Materials/ IMMM95, Ed: Tokuda M., 1995, Tsinghua Univ., Beijing.

[2] Aifantis E.C., Preliminaries on degradation and chemomechanics. NSF Workshop on a Continuum Mechanics Approach to Damage and Life Prediction, Ed: Stouffer D.C., Krempl E., Fitzgerald J.E., 1980, 159-173, Carrolton.

[3] Aifantis E.C., On the role of gradients in the localization of deformation and fracture, Int. J. Eng. Sci., 1992, 30, 1279-1299.

[4] Aifantis E.C., Internal length gradient (ILG) material mechanics across scales and disciplines, Adv. App. Mech. 2016, 49, 1-110.

[5] Aifantis E.C., On the problem of diffusion in solids, Acta Mech., 1980, 37, 265-296.

[6] Aifantis E.C., Gradient nanomechanics: Applications to deformation, fracture, and diffusion in nanopolycrystals, Metall. Mater. Trans. A, 2011, 42, 2985-2998.

[7] Tsagrakis I., Aifantis E.C., Thermodynamic coupling between gradient elasticity and a Cahn-Hilliard type of diffusion: Size dependent spinodal gaps, Continuum Mech. Therm., 2017, 29(6), 1181-1194.

[8] Tsagrakis I., Aifantis E.C., Gradient and size effects on spinodal and miscibility gaps, Continuum Mech. Therm., 2018, 30(5), 1185-1199.

[9] Tsagrakis I., Aifantis E.C., Gradient elasticity effects on the two-stage lithiation of LIB anodes, In: Generalized Models and Non-Classical Approaches in Complex Materials 2, Adv. Struct. Mater., Springer, Ed:. Altenbach H., Pouget J., Rousseau M., Collet B., Michelitsch T., 2018, 90, 221-235.

[10] Tsagrakis I., Yasnikov I.S., Aifantis E.C., Gradient elasticity for disclinated micro crystals. Mech. Res. Commun. 2018, 93, 159-162.

[11] Cahn J.W., Hilliard J.E., Free energy of a nonuniform system. I. Interfacial free energy, J. Chem. Phys., 1958, 28, 258-267; Free energy of a nonuniform system. II. Thermodynamic Basis, J. Chem. Phys. 1959, 30, 1121-1124.

[12] Unger D.J., Gerberich W.W., Aifantis E.C., Further remarks on the implications of steady state stress assisted diffusion on environmental cracking, Scripta Metall., 1982, 16, 1059-1064.

[13] Qu R.T., Zhang Z.F., A universal fracture criterion for high-strength materials, Sci. Rep., 2013, 3, 1117.

[14] K. Zhao, W.L. Wang, J. Gregoire, M. Pharr, Z. Suo, J.J. Vlassak and E. Kaxiras, Lithium-assisted plastic deformation of silicon electrodes in lithium-ion batteries: A first-principles theoretical study, Nano Lett., 2011, 11, 2962-2967.

[15] Moon J., Cho K., Cho M., Ab-initio study of silicon and tin as a negative electrode materials for lithium-ion batteries, Int. J. Precis. Eng. Man., 2012, 13, 1191-1197.
[16] Gryaznov V.G., Kaprelov A.M., Polonskii I.A., Romanov A.E., Disclinations in heterogeneous small particles, Phys. Status Solidi, 1991, 167, 29-36.
[17] Bagni C., Askes H., Aifantis E.C., Gradient-enriched finite element methodology for axisymmetric problems, Acta Mech., 2017, 228, 1423-1444.
[18] Askes H., Aifantis E.C., Gradient elasticity in statics and dynamics: an overview of formulations, length scale identification procedures, finite element implementations and new results, Int. J. Solids Struct., 2011, 48, 1962-1990.
[19] Polizzotto C., Stress gradient versus strain gradient constitutive models within elasticity, Int. J. Solids Struct., 2014, 51, 1809-1818.
[20] Yasnikov I.S., Vikarchuk A.A., Voids in icosahedral small particles of an electrolytic metal, JETP Letters, 2006, 83, 42-45.
[21] Howie A., Marks L.D., Elastic strains and the energy balance for multiply twinned particles, Philos. Mag. A, 1984, 49, 95-109.
[22] Aifantis K.E., Brutti S., Hackney S.A., Sarakonsri T., Scrosati B., SnO2/C nanocomposites as anodes in secondary Li-ion batteries, Electrochim. Acta, 2010, 55, 5071-5076.
[23] Aifantis K.E., Huang T., Hackney S.A., Sarakonsri T., Yu A., Capacity fade in Sn-C nanopowder anodes due to fracture, J. Power Sources, 2012, 197, 246-252.
[24] Aifantis E.C., Towards internal length gradient chemomechanics, Rev. Adv. Mater. Sci., 2017, 48, 112-130.